Japanese Journal of Applied Physics
Vol. 45, No. 36, 2006, pp. L980–L983

Experimental Study of Detectable Sizes of Surface Flaws on Copper Tubes by Nondestructive Inspection Using High-T_c Superconducting Quantum Interference Device

Yoshimi HATSUKADE*, Shinya OKUNO, Kazuaki MORI[1] and Saburo TANAKA

Toyohashi University of Technology, 1-1 Hibarigaoka, Tempaku-cho, Toyohashi, Aichi 441-8580, Japan
[1]*Sumitomo Light Metal Industries, Ltd., Copper Works, 100 Ougishinmichi, Ichinomiya-cho, Hoi-gun, Aichi 441-1295, Japan*

(Received July 11, 2006; accepted July 30, 2006; published online September 8, 2006)

Detectable sizes of shallow flaws on thin copper tubes were experimentally investigated using an eddy-current-based nondestructive inspection system with a high-T_c superconducting quantum interference device (SQUID) gradiometer. At an excitation field of 5.6 μT at 3 kHz, a magnetic anomaly due to the shallowest flaw of 10 μm depth, 100 μm width, and 15 mm length on the surface of a tube specimen of 6.35 mm outer diameter and 0.8 mm thickness was successfully measured. Signal amplitude due to a flaw was proportional to effective flaw volume that made an induced eddy current detour. The experimental results indicate that the detectable volume of a surface flaw on a copper tube should be 1×10^6 μm^3 with some increase in signal-to-noise ratio. [DOI: 10.1143/JJAP.45.L980]

KEYWORDS: copper tube, surface flaw, detectable flaw size, high-T_c SQUID gradiometer, eddy current

Copper tubes have been employed as heat-exchanger tubes in air conditioners, among others. For higher performance and for economical and ecological reasons, the thickness of the copper heat-exchanger tubes has been reduced to less than 1 mm. During the fabrication of such tubes, small flaws accidentally occur on tube surfaces. The flaws become elongated and thin with the reduction in the thickness of the tubes, and finally become shallow and long. Recently, shallow surface flaws of less than 50 μm depth have brought about tube breakage in bending or flaring postprocesses. However, it is difficult to detect such shallow flaws on tube surfaces by conventional nondestructive inspection (NDI) techniques such as eddy current testing (ECT) and ultrasonic testing (UT).[1–3]

We previously presented a novel NDI technology using high-T_c superconducting quantum interference devices (SQUIDs) to detect shallow flaws on metallic tubes.[4,5] Taking advantage of SQUIDs' uncontested magnetic sensitivity, the NDI technique is applied to the detection of surface flaws of less than 50 μm depth on thin copper tubes. In this study, we experimentally evaluated the capability of the technique in inspecting of flaws of various sizes on thin copper tubes.

We have constructed an eddy-current-based SQUID-NDI system that employs a Helmholtz-coil-type inducer and a high-T_c SQUID gradiometer.[6] Figure 1 shows a schematic diagram of the system. The planar direct-coupled-type SQUID gradiometer has a differential pickup coil. The area of one of rectangular pickup coils and the length of the baseline are 5.5×3.6 mm^2 and 3.6 mm, respectively. The magnetic flux noise of the SQUID-NDI system measured in a flux-locked loop operation without magnetic shielding is about 15 $\mu\phi_0$/Hz$^{1/2}$ between 100 Hz and 20 kHz, where $\phi_0 = 2.07 \times 10^{-15}$ Wb is the magnetic flux quantum. The SQUID is set in a fiber reinforced plastic (FRP) cryostat with liquid nitrogen inside. Two winding coils form the Helmholtz-coil-type field inducer. The turn number and dimensions of each coil are 1000, and 48 mm in diameter and 45 mm in length, respectively. The field coils are set on the same axis with a distance of 36 mm between each coil end. An electric motor moves a copper tube specimen on a rail through the inducer at a velocity of up to 25 mm/s. An ac field generated by the inducer induces an eddy current in the copper tube under test. A lock-in amplifier measures the output voltage from the SQUID electronics. A data logger records the output data from the lock-in amplifier on a personal computer (PC).

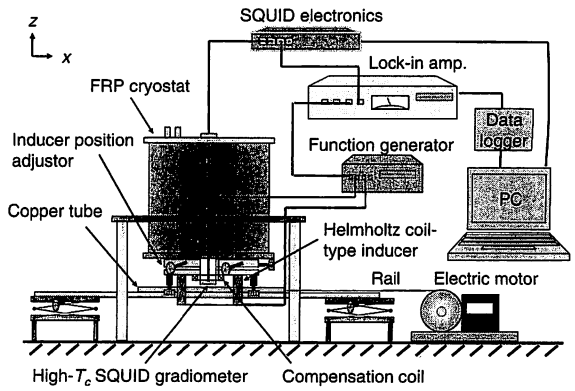

Fig. 1. Schematic diagram of eddy-current-based SQUID-NDI system for tube inspection using high-T_c SQUID gradiometer and Helmholtz-coil-type inducer.

We prepared copper tube specimens of 6.35 mm outer diameter, 0.8 mm thickness, and 300 mm length, which were selected from industrial products, with a wide range of flaw sizes. We define the depth, width, and length of a flaw as shown schematically in Fig. 2. The flaws range from 10 to 100 μm in depth, 50–200 μm in width, and 2–25 mm in length. The flaw sizes of each specimen are summarized in Table I. These values were set in an electric discharge machine, which made the flaws on the copper tubes. The values were confirmed using polymers that replicated the flaws.

We inspected the tube specimens with an excitation field B_x of 5.6 μT at 3 kHz at the center between the field coils (see Fig. 1). We selected the frequency of 3 kHz according to the previous results.[4,5] The tube specimens were passed

*Corresponding author. E-mail address: hatukade@eco.tut.ac.jp

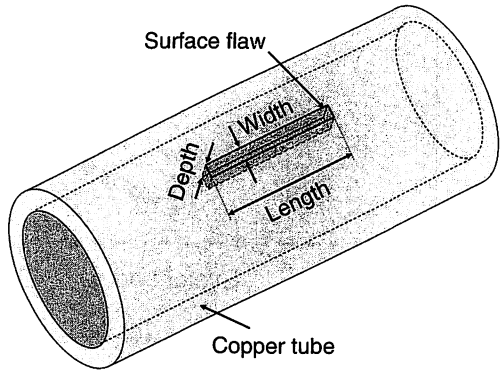

Fig. 2. Schematic illustration of surface flaw on copper tube. The flaw depth, width, and length are described.

Table I. Dimensions of surface flaws.

Specimen	Depth (μm)	Width (μm)	Length (mm)
A	100	100	15
B	50	100	15
C	50	100	10
D	50	100	5
E	50	100	2
F	50	50	15
G	30	100	15
H	20	200	25
I		100	
J	10	100	15

through the inducer at 10 mm/s. The flaws on the specimens were oriented to be closest to the SQUID gradiometer. The liftoff distance (the shortest distance between the gradiometer and the tube specimen) was 3 mm. The SQUID gradiometer measured the gradient in the x-direction (parallel to the tube axis) of the vertical magnetic flux density, dB_z/dx. The position of the inducer was carefully adjusted relative to the SQUID to minimize the SQUID output due to the excitation field by itself. A compensation coil, which was located near the SQUID, compensated for the remaining leak excitation flux coupled to the SQUID using current with the same frequency as that of the excitation field. The sampling frequency of the data logger was 100 Hz, which corresponds to a sampling space of 0.1 mm.

Typical measurement results of the tube specimens B with a 50-μm-depth flaw and J with a 10-μm-depth flaw are shown in Figs. 3(a) and 3(b), respectively. Both flaws are 100 μm in width and 15 mm in length. In each figure, a pair of thick arrows pointing up denotes the positions of the flaw ends. As shown in Fig. 3(a), two pairs of upward and downward peaks, which are close to each other such that the edges of the downward peaks are overlapping, are observed at both flaw ends. Since the positions of the flaw ends are known in these waveforms, we can extract a flaw signal and its peak-to-peak amplitude that is denoted by a double-edged thin arrow between dashed lines in the midst of a flaw, as shown in Figs. 3(a) and 3(b), respectively. Even an anomalous magnetic signal due to the shallowest 10-μm-depth flaw was successfully detected near the flaw. The

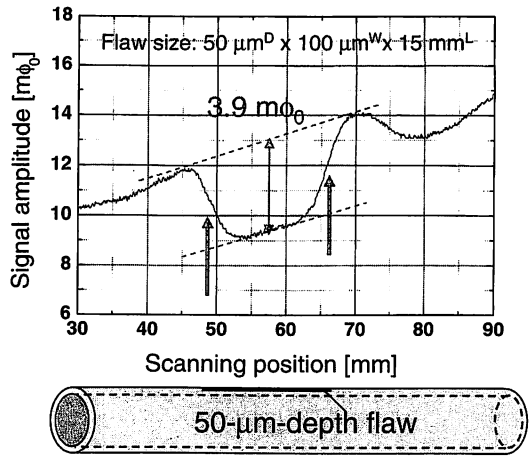

(a)

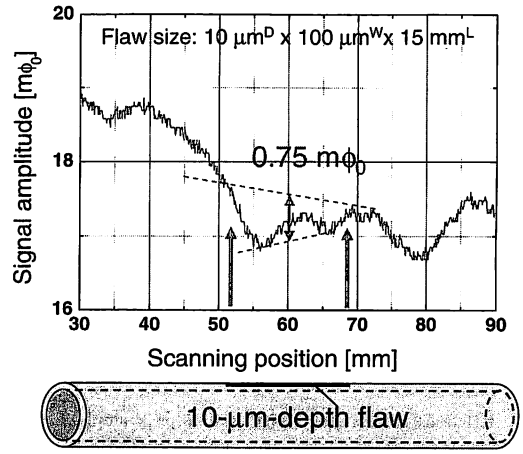

(b)

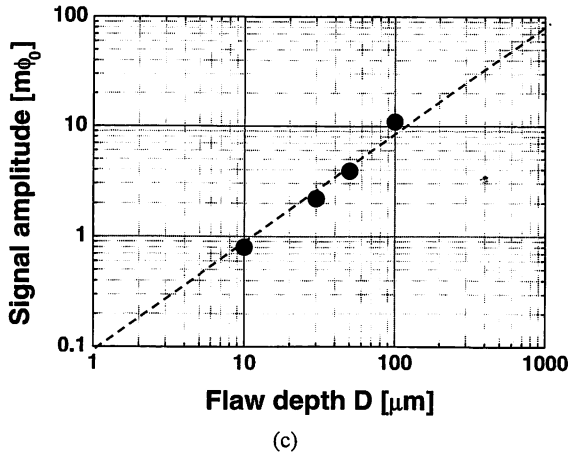

(c)

Fig. 3. Experimental results of different-depth flaws with width of 100 μm and length of 15 mm: (a) 50-μm-depth flaw, (b) 10-μm-depth flaw. (c) Signal peak-to-peak amplitude due to flaw as function of flaw depth D. In (a) and (b), a pair of thick arrows pointing up denote positions of flaw ends.

slanting offsets observed in these figures are due to the edge effects because these flaws were not located at the center of the tube specimens.[4] In the case of the flaw located at the center of the specimens, no slanting offset was observed. The signal peak-to-peak amplitude of J is about 5 times

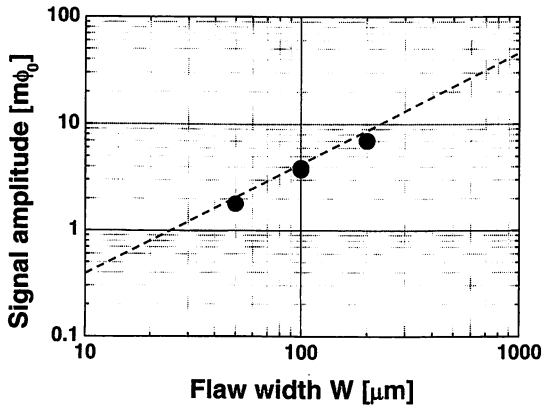

(a)

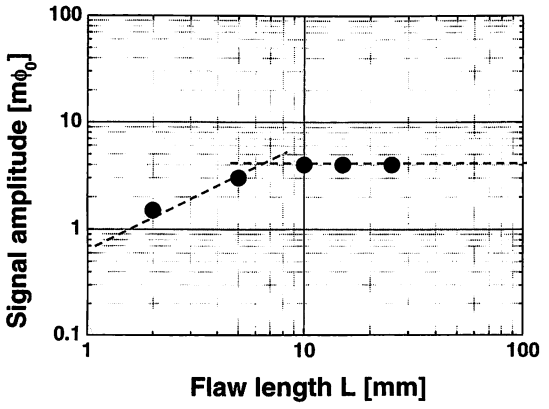

(b)

Fig. 4. Relationships between signal peak-to-peak amplitudes and other flaw parameters. (a) Flaw width *W*. (b) Flaw length *L*.

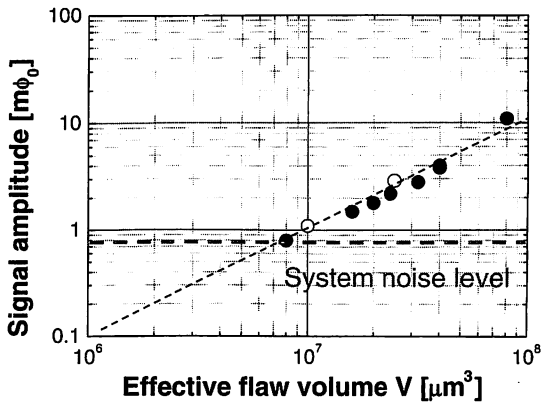

(a)

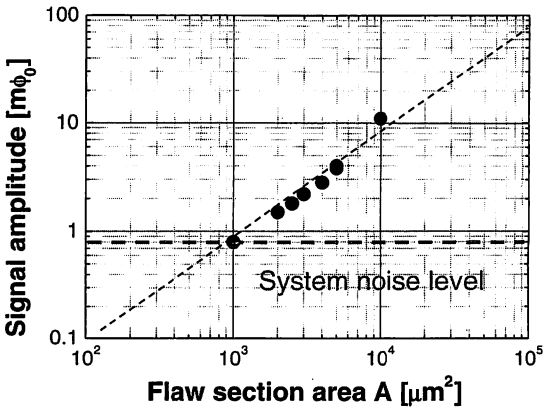

(b)

Fig. 5. Relationships between signal peak-to-peak amplitudes and flaw parameters. (a) Effective flaw volume *V*. The signal amplitudes due to flaws greater than 8 mm in length are denoted by closed circles, whereas the other amplitudes are denoted by open circles. (b) Flaw section area *A*. The horizontal dashed lines show system noise levels.

smaller than that of B. Figure 3(c) shows the relationship between flaw depth and signal amplitude, which were obtained from the results of specimens A, B, G, and J. Signal amplitude is proportional to flaw depth, for the same flaw width and length.

Figure 4(a) shows the relationship between signal amplitude and flaw width. It was obtained from the results of specimens B and F with a flaw depth of 50 μm, and H and I with a flaw depth of 20 μm. The signal amplitudes of H and I are normalized to the amplitudes of the flaw depth of 50 μm, in accordance with the above-mentioned depth dependence. Signal amplitude is proportional to flaw width for the same flaw depth, although it was not normalized with length.

Figure 4(b) shows the relationship between flaw length and signal amplitude, which were obtained from the results of specimens B, C, D, E, and I. The result of specimen I is normalized only with depth. When the flaw length is larger than about 8 mm, signal amplitude is constant, when the length is smaller, signal amplitude is proportional to flaw length, for the same flaw depth and width. This length dependence can be explained as follows, considering the fact that the current passing under a flaw does not contribute to the anomalous magnetic signal. In the case of a long flaw, the eddy current induced near flaw ends should be partially detoured near the flaw, and the remaining current should pass under the flaw, whereas the current induced in the vicinity of the middle of the flaw should mostly pass under the flaw. The signal amplitude curve indicates that the currents induced within about 4 mm from flaw ends can be detoured.

The experimental results were rearranged to clarify the dependences of signal amplitude on flaw volume and flaw section area. Figure 5(a) shows the flaw volume dependence on signal amplitude for flaw lengths both greater and less than 8 mm. Figure 5(b) shows the flaw section area dependence on signal amplitude for flaw length greater than 8 mm. In Fig. 5(a), we used effective flaw volume when the real flaw length was greater than 8 mm. This means that the volume in this case is calculated from the product of depth, width, and 8 mm length. The signal amplitudes due to the flaws greater than 8 mm in length are denoted by closed circles, whereas the other amplitudes are denoted by open circles. Figure 5(b) shows the section area calculated from the product of depth and width. The signal amplitudes in both graphs are highly proportional to volume and section area. The noise levels of the NDI system are also shown in these figures. The minimum detectable flaw by the system is the flaw with a volume of approximately 8×10^6 μm^3 or a section area of 1×10^3 μm^2 when the length is greater than 8 mm.

Signal amplitude depends on liftoff distance, excitation

field strength, and frequency. The system noise is mainly attributable to the HTS-SQUID. The signal-to-noise ratio is increased by applying a strong excitation field. However, a strong excitation field often induces flux trapping. The development of a high-performance high-T_c SQUID with low noise and robustness to a strong excitation field increases the potential of the NDI system. A system noise of $0.1\,m\phi_0$ and a liftoff distance of 1.5 mm decrease the detectable volume to $1 \times 10^6\,\mu m^3$, or the section area to $250\,\mu m^2$ when the flaw is greater than 8 mm. According to the refs. 2 and 3, the detectable flaw size produced by conventional methods (UT and ECT) is estimated to be about $1 \times 10^7\,\mu m^3$; in particular, the detectable flaw depth is limited to about 50 μm. Therefore, by increasing signal-to-noise ratio, the SQUID-NDI technique should show an advantage of detecting shallower flaws on metallic tubes. Improvements in optimizing the system parameters are in progress.

In summary, the minimum detectable size of a surface flaw on a copper tube is approximately $8 \times 10^6\,\mu m^3$ in flaw volume or $1 \times 10^3\,\mu m^2$ in flaw section area when the flaw length is greater than 8 mm, determined using the present SQUID-NDI system. By improving the SQUID characteristics and optimizing the system parameters, it is possible to detect shallow long flaws on copper tubes such as those of 5 μm depth and 40 μm width, or 2 μm depth and 100 μm width.

The authors would like to thank Dr. Naoko Kasai, AIST, Japan, for helpful discussions.

1) A. J. Trivedi and R. R. Parikh: Proc. 14th World Conf. Non-Destructive Testing, 1996, Vol. 3, p. 1729.
2) K. A. Gopal, N. Raghu, N. G. Muralidharan, P. V. Kumar and K. V. Kasiviswanathan: Proc. 14th World Conf. Non-Destructive Testing, 1996, Vol. 2, p. 663.
3) A. Fedorov, V. Popov, V. Gorsky and A. A. Bochvar: Proc. 14th World Conf. Non-Destructive Testing, 1996, Vol. 3, p. 1709.
4) Y. Hatsukade, A. Kosugi, K. Mori and S. Tanaka: Jpn. J. Appl. Phys. **43** (2004) L1488.
5) Y. Hatsukade, A. Kosugi, K. Mori and S. Tanaka: Physica C **426–431** (2005) 1585.
6) Y. Hatsukade, A. Kosugi, N. Ishizaka, S. Okuno, K. Mori and S. Tanaka: Supercond. Sci. Technol. **19** (2006) S149.